

Next-ViT: Next Generation Vision Transformer for Efficient Deployment in Realistic Industrial Scenarios

Jiashi Li*, Xin Xia*[†], Wei Li*, Huixia Li, Xing Wang,
Xuefeng Xiao, Rui Wang, Min Zheng, Xin Pan
ByteDance Inc

{lijiashi, xiaxin.97, liwei.97, lihuixia, wangxing.613}@bytedance.com
{xiaoxuefeng.ailab, ruiwang.rw, zhengmin.666, panxin.321}@bytedance.com

Abstract

Due to the complex attention mechanisms and model design, most existing vision Transformers (ViTs) can not perform as efficiently as convolutional neural networks (CNNs) in realistic industrial deployment scenarios, e.g. TensorRT and CoreML. This poses a distinct challenge: Can a visual neural network be designed to infer as fast as CNNs and perform as powerful as ViTs? Recent works have tried to design CNN-Transformer hybrid architectures to address this issue, yet the overall performance of these works is far away from satisfactory. To end these, we propose a next generation vision Transformer for efficient deployment in realistic industrial scenarios, namely Next-ViT, which dominates both CNNs and ViTs from the perspective of latency/accuracy trade-off. In this work, the Next Convolution Block (NCB) and Next Transformer Block (NTB) are respectively developed to capture local and global information with deployment-friendly mechanisms. Then, Next Hybrid Strategy (NHS) is designed to stack NCB and NTB in an efficient hybrid paradigm, which boosts performance in various downstream tasks. Extensive experiments show that Next-ViT significantly outperforms existing CNNs, ViTs and CNN-Transformer hybrid architectures with respect to the latency/accuracy trade-off across various vision tasks. On TensorRT, Next-ViT surpasses ResNet by 5.4 mAP (from 40.4 to 45.8) on COCO detection and 8.2% mIoU (from 38.8% to 47.0%) on ADE20K segmentation under similar latency. Meanwhile, it achieves comparable performance with CSWin, while the inference speed is accelerated by 3.6x. On CoreML, Next-ViT surpasses EfficientFormer by 4.6 mAP (from 42.6 to 47.2) on COCO detection and 3.5% mIoU (from 45.2% to 48.7%) on ADE20K segmentation under similar latency. Code will be released recently.

*Equal contribution.

[†]Corresponding author.

1. Introduction

Recently, vision Transformers (ViTs) have received increasing attention in industry and academia, and demonstrated much success in various computer vision tasks, such as image classification, object detection, semantic segmentation and etc. However, CNNs still dominate vision tasks from a real-world deployment perspective, because ViTs are usually much slower than classical CNNs, e.g. ResNets. There are some factors that limit the inference speed of the Transformer model, including quadratic complexity with respect to token length of the Multi-Head Self Attention (MHSA) mechanism, non-foldable LayerNorm and GELU layers, the complex model design causes frequent memory access and copying, etc.

Many works have struggled to free ViTs from high latency dilemma. For example, Swin Transformer [20] and PVT [35] try to design more efficient spatial attention mechanisms to alleviate the quadratic-increasing computation complexity of MHSA. The others [4, 18, 24] consider combining efficient convolution blocks and powerful Transformer blocks to design CNN-Transformer hybrid architecture to obtain a better trade-off between accuracy and latency. Coincidentally, almost all existing hybrid architectures [4, 18, 24] adopt convolution blocks in the shallow stages and just stack Transformer block in the last few stages. However, we observe that such a hybrid strategy is effortless to lead to performance saturation on downstream tasks (e.g. segmentation and detection). Furthermore, we found that both convolution blocks and Transformer blocks in existing works can not possess characteristics of efficiency and performance at the same time. Although the accuracy-latency trade-off has been improved when compared with Vision Transformer, the overall performance of the existing hybrid architecture is still far away from satisfactory.

To address the above issues, this work develops three important components to design efficient vision Transformer

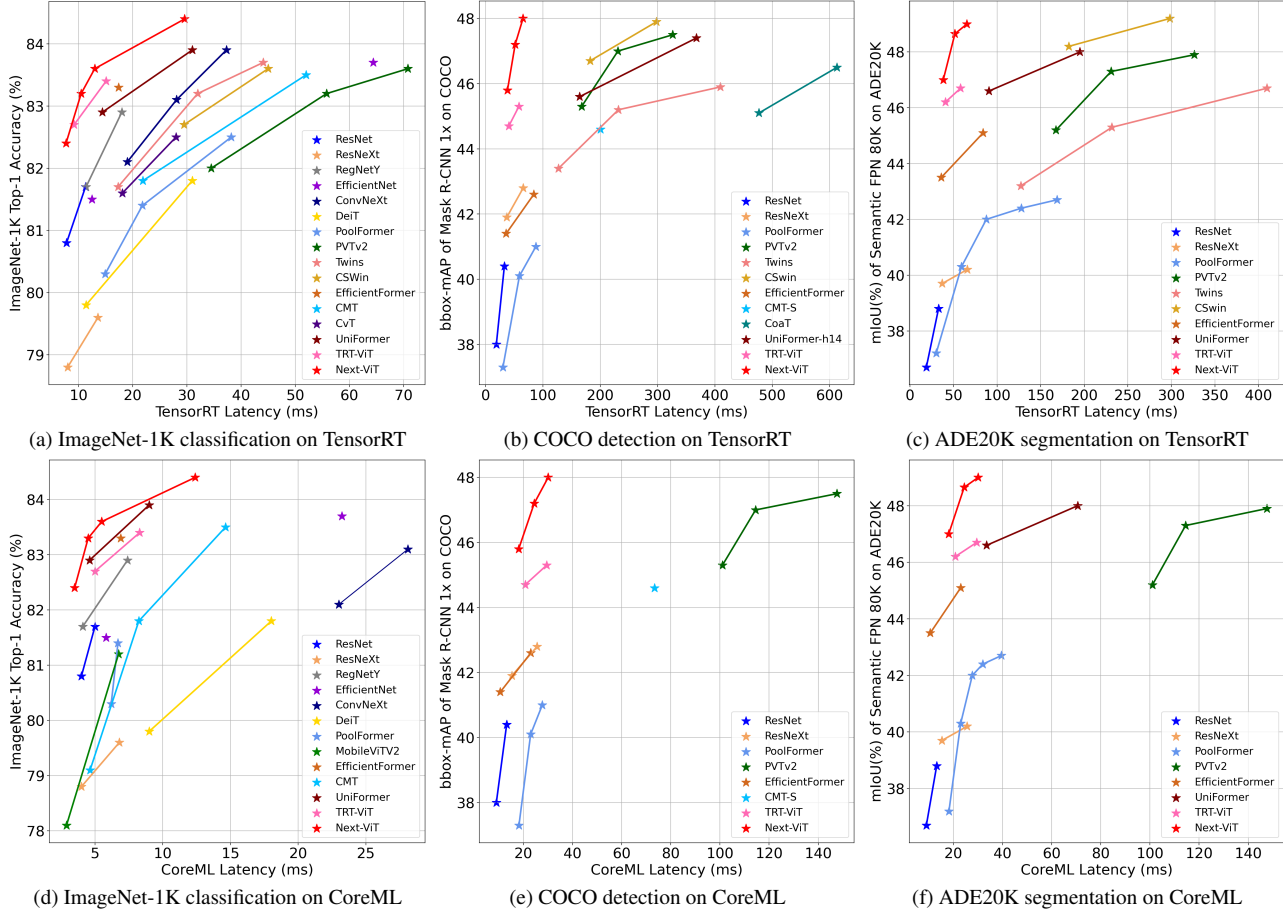


Figure 1. Comparison among Next-ViT and efficient Networks, in terms of accuracy-latency trade-off.

networks. Firstly, we introduce the Next Convolution Block (NCB), which is skilled at capturing short-term dependency information in visual data with a novel deployment-friendly Multi-Head Convolutional Attention (MHCA). Secondly, we build the Next Transformer Block (NTB), NTB is not only an expert in capturing long-term dependency information but also works as a lightweight and high-and-low-frequency signal mixer to enhance modeling capability. Finally, we design Next Hybrid Strategy (NHS) to stack NCB and NTB in a novel hybrid paradigm in each stage, which greatly reduce the proportion of the Transformer block and retaining the high precision of the vision Transformer network in various downstream tasks.

Based on the above-proposed approaches, we propose next generation vision Transformer for realistic industrial deployment scenarios (abbreviated as Next-ViT). In this paper, to present a fair comparison, we provide a view that treats the latency on the specific hardware as direct efficiency feedback. TensorRT and CoreML represent generic and easy-to-deploy solutions for server-side and mobile-side devices, respectively, that help provide convincing

hardware-oriented performance guidance. With this direct and accurate guidance, we redraw the accuracy and latency trade-off diagram of several existing competitive models in Figure 1. As depicted in Figure 1(a)(d), Next-ViT achieves best latency/accuracy trade-off on ImageNet-1K classification task. More importantly, Next-ViT shows a more significant latency/accuracy trade-off superiority on downstream tasks. As shown in Figure 1(b)(c), on TensorRT, Next-ViT outperforms ResNet by **5.4** mAP (from 40.4 to 45.8) on COCO detection and **8.2%** mIoU (from 38.8% to 47.0%) on ADE20K segmentation under similar latency. Next-ViT achieves comparable performance with CSWin, while the inference speed is increased by **3.6x**. As depicted in Figure 1(e)(f), on CoreML, Next-ViT surpass EfficientFormer by **4.6** mAP (from 42.6 to 47.2) on COCO detection and **3.6%** mIoU (from 45.2% to 48.7%) on ADE20K segmentation under similar CoreML latency.

Our main contributions are summarized as follows:

- We develop powerful convolution block and Transformer block, i.e. NCB and NTB, with deployment-friendly mechanisms. Next-ViT stacks NCB and NTB

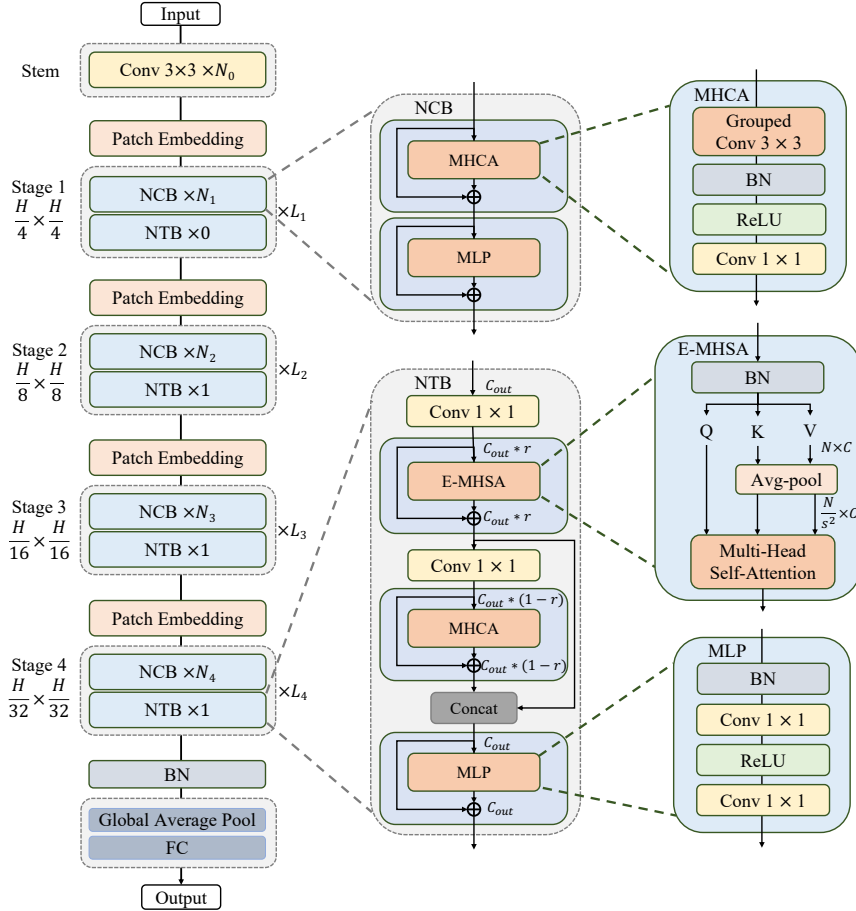


Figure 2. The left column is the overall hierarchical architecture of Next-ViT. The medium column are the Next Convolution Block (NCB) and the Next Transformer Block (NTB). The right column are the detailed visualization of multi-head convolutional attention (MHCA), efficient multi-head self-attention (E-MHSA) and the optimized MLP modules.

to build advanced CNN-Transformer hybrid architecture.

- We design an innovative CNN-Transformer hybrid strategy from a new insight that boosts performance with high efficiency.
- We present Next-ViT, a family of powerful vision Transformer architecture. Extensive experiments demonstrate the advantage of Next-ViT. It achieves SOTA latency/accuracy trade-off on image classification, object detection and semantic segmentation on TensorRT and CoreML.

We believe that our work builds a stable bridge between academic research and industrial deployment in terms of visual neural network design. We hope that our work will provide new insights and promote more research in neural network architecture design for practical industrial deployment.

2. Related Work

Convolutional Networks. Over the past decade, Convolutional Neural Networks (CNNs) have dominated vision architectures in a variety of computer vision tasks, including image classification, object detection, and semantic segmentation. ResNet [9] uses residual connections to eliminate network degradation, ensuring that the network builds deeper and can capture high-level abstractions. DenseNet [12] alternately enhances feature reuse and concatenates feature maps through dense connections. MobileNets [11, 29] introduce depthwise convolution and point-wise convolution to build models with small memory and low latency. ShuffleNet [44] adopts group point-wise convolution and channel shuffle to reduce the computational cost further. ShuffleNetv2 [23] propose that network architecture design should consider the direct metric such as speed, instead of the indirect metric like FLOPs. ConvNeXt [21] reviews the design of the vision Transform-

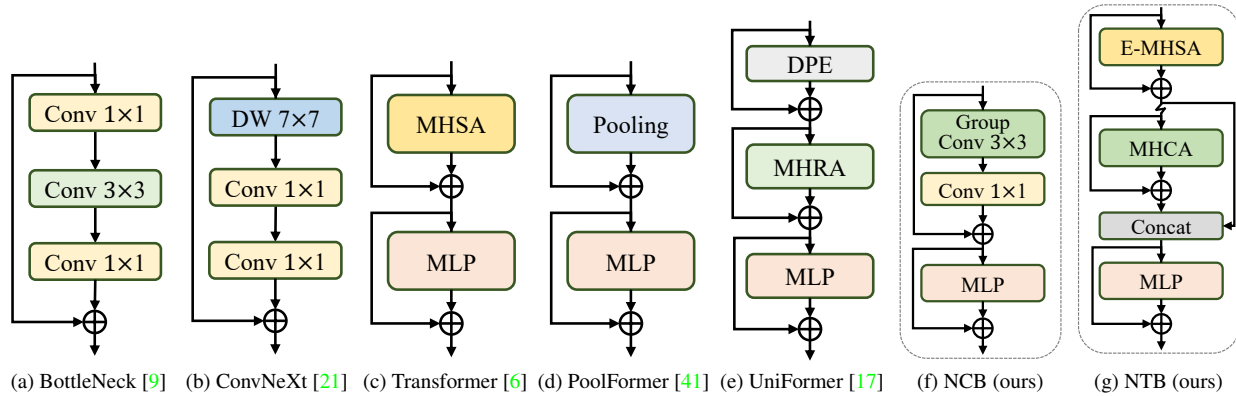


Figure 3. Comparison of different Transformer-based and convolution-based blocks.

ers and proposes a pure CNN model that can compete favorably with SOTA hierarchical vision Transformers across multiple computer vision benchmarks, while retaining the simplicity and efficiency of standard CNNs.

Vision Transformers. Transformer is first proposed in the field of natural language processing (NLP). ViT [6] splits the image into patches and treats these patches as words to perform self-attention, which shows that Transformer also achieves impressive performance on various vision tasks. DeiT [32] introduces a teacher-student strategy specific to Transformers. T2T-ViT [42] introduces a novel tokens-to-token (T2T) process to progressively tokenize images to tokens and structurally aggregate tokens. Swin Transformer [20] proposes a general-purpose Transformer backbone, which constructs hierarchical feature maps and has linear computational complexity to image size. PiT [10] incorporates a pooling layer into ViT, and shows that these advantages can be well harmonized to ViT through extensive experiments. Today, researchers pay more attention to efficiency, including efficient self-attention, training strategy, pyramid design, and etc.

Hybrid Models. Recent works [7, 18, 24, 30, 36] have shown that combining convolution and Transformer as a hybrid architecture helps absorb the strengths of both architectures. BoTNet [30] replaces the spatial convolutions with global self-attention in the final three bottleneck blocks of ResNet. CvT [36] introduces the depthwise and pointwise convolution in front of self-attention. CMT [7] proposes a new Transformer based hybrid network by taking advantage of Transformers to capture long-range dependencies and CNN to model local features. In MobileViT [24], introduces a light-weight and general-purpose vision Transformer for mobile devices. MobileFormer [2] combines with the proposed lightweight cross attention to model the bridge, which is not only computationally efficient, but also has more representation power. EfficientFormer [18] complies with a dimension consistent design that smoothly

leverages hardware-friendly 4D MetaBlocks and powerful 3D MHSA blocks. In this paper, we design a family of Next-ViT models that adapt more to the realistic industrial scenarios.

3. Methods

In this section, we first demonstrate the overview of the proposed Next-ViT. Then, we discuss some core designs within Next-ViT, including the Next Convolution Block (NCB), Next Transformer Block (NTB) and the Next Hybrid Strategy (NHS). Moreover, we provide the architecture specifications with different model sizes.

3.1. Overview

We present the Next-ViT as illustrated in Figure 2. By convention, Next-ViT follows the hierarchical pyramid architecture equipped with a patch embedding layer and a series of convolution or Transformer blocks in each stage. The spatial resolution will be progressively reduced by $32\times$ while the channel dimension will be expanded across different stages. In this chapter, we first dive deeper into designing the core blocks for information interaction and respectively develop powerful NCB and NTB to model short-term and long-term dependencies in visual data. The fusion of local and global information is also performed in NTB which further boosts modeling capability. Finally, we systematically study the manners of integrating convolution and Transformer blocks. To overcome the inherent defects of existing methods, we introduce Next Hybrid Strategy which stacks innovative NCB and NTB to build our advanced CNN-Transformer hybrid architecture.

3.2. Next Convolution Block (NCB)

To present the superiority of the proposed NCB, we first revisit some classical structural designs of convolution and Transformer blocks as shown in Figure 3. BottleNeck block proposed by ResNet [9] has dominance in visual neural

networks for a long time by its inherent inductive biases and deployment-friendly characteristics in most hardware platforms. Unfortunately, the effectiveness of the BottleNeck block is unsatisfactory compared to the Transformer block. ConvNeXt block [21] modernizes the BottleNeck block by imitating designs of Transformer block. While ConvNeXt block partly improves network performance, its inference speed on TensorRT/CoreML is severely limited by inefficient components, such as 7×7 depthwise convolution, LayerNorm, and GELU. Transformer block has achieved excellent results in the various visual task and its intrinsic superiority is jointly endowed by the paradigm of MetaFormer [41] and the attention-based token mixer module [20] [5]. However, the inference speed of Transformer block is much slower than BottleNeck block on TensorRT and CoreML due to its complex attention mechanisms, which is unbearable in most realistic industrial scenarios.

To overcome the defeats of the above blocks, we introduce a Next Convolution Block (NCB), which maintains the deployment advantage of BottleNeck block while obtaining prominent performance as Transformer block. As shown in Figure 3(f), NCB follows the general architecture of MetaFormer [41], which is verified to be essential to the Transformer block. In the meantime, an efficient attention-based token mixer is equally important. We design a novel Multi-Head Convolutional Attention (MHCA) as an efficient token mixer with deployment-friendly convolution operation. Finally, we build NCB with MHCA and MLP layer in the paradigm of MetaFormer [41]. Our proposed NCB can be formulated as follows:

$$\begin{aligned} \tilde{z}^l &= \text{MHCA}(z^{l-1}) + z^{l-1} \\ z^l &= \text{MLP}(\tilde{z}^l) + \tilde{z}^l \end{aligned} \quad (1)$$

where z^{l-1} denotes the input from the $l-1$ block, \tilde{z}^l and z^l are the outputs of MHCA and the l NCB. We will introduce MHCA in detail in the next section.

3.2.1 Multi-Head Convolutional Attention (MHCA)

To free the existing attention-based token mixer from the high latency dilemma, we design a novel attention mechanism with efficient convolution operation, i.e. Convolutional Attention (CA), for fast inference speed. In the meantime, inspired by the effective multi-head design in MHSA [33], we build our convolutional attention with multi-head paradigm which jointly attend to information from different representation subspaces at a different position for effective local representation learning. The definition of proposed Multi-Head Convolutional Attention (MHCA) can be summarized as follows:

$$\text{MHCA}(z) = \text{Concat}(\text{CA}_1(z_1), \text{CA}_2(z_2), \dots, \text{CA}_h(z_h))W^P \quad (2)$$

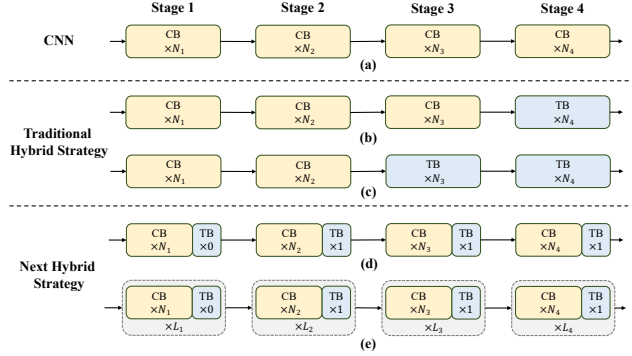


Figure 4. Comparison of traditional hybrid strategies and NHS.

Here, MHCA captures information from h parallel representation subspaces. To promote the information interaction across the multiple heads, we also equip MHCA with a projection layer (W^P). $z = [z_1, z_2, \dots, z_h]$ indicates to divide the input feature z into multi-head form in channel dimension. CA is single-head convolutional attention which can be defined as:

$$\text{CA}(z) = \text{O}(W, (T_m, T_n)) \text{ where } T_{\{m,n\}} \in z \quad (3)$$

where T_m and T_n are adjacent tokens in input feature z . O is an inner product operation with trainable parameter W and input tokens $T_{\{m,n\}}$. CA is capable of learning affinity between different tokens in the local receptive field through iteratively optimizing trainable parameter W . Concretely, the implementation of MHCA is carried out with a group convolution (multi-head convolution) and a point-wise convolution, as shown in Figure 3(f). We uniformly set head dim to 32 in all MHCA for fast inference speed with various data-type on TensorRT. Besides, we adopt efficient Batch-Norm (BN) and ReLU activation function in NCB rather than LayerNorm (LN) and GELU in traditional Transformer blocks, which further accelerates inference speed. Experimental results in the ablation study show the superiority of NCB compared with existing blocks, e.g BottleNeck block, ConvNext block, LSA block and etc.

3.3. Next Transformer Block (NTB)

Although the local representation has been effectively learned via NCB, the capture of global information is urgent to be addressed. Transformer block has a strong ability to capture low-frequency signals which provide global information (e.g global shapes and structures). Nevertheless, relevant studies [26] have observed that Transformer blocks may deteriorate high-frequency information, such as local textures information, to a certain extent. Signals in different frequency segments are indispensable in the human visual system [1] [15] and will be fused in some specific way to extract more essential and distinct features.

Motivated by these observations, we develop the Next Transformer Block (NTB) to capture multi-frequency signals in the lightweight mechanism. Furthermore, NTB works as an effective multi-frequency signals mixer to further enhance overall modeling capability. As shown in Figure 2, NTB firstly captures low-frequency signals with an Efficient Multi-Head Self Attention(E-MHSA) which can be depicted as:

$$\text{E-MHSA}(z) = \text{Concat}(\text{SA}_1(z_1), \text{SA}_2(z_2), \dots, \text{SA}_h(z_h))W^P \quad (4)$$

where $z = [z_1, z_2, \dots, z_h]$ denotes to divide the input feature z into multi-head form in channel dimension. SA is a spatial reduction self-attention operator which is inspired by Linear SRA [34] and performing as:

$$\text{SA}(X) = \text{Attention}(X \cdot W^Q, \text{P}_s(X \cdot W^K), \text{P}_s(X \cdot W^V)) \quad (5)$$

where Attention represents a standard attention calculating as $\text{Attention}(Q, K, V) = \text{softmax}(\frac{QK^T}{d_k})V$, in which d_k denotes the scaling factor. W^Q, W^K, W^V are linear layers for context encoding. P_s is an avg-pool operation with stride s for downsampling the spatial dimension before the attention operation to reduce computational cost. Specifically, We observe the time consumption of the E-MHSA module is also greatly affected by its number of channels. NTB thus performs a channel dimension reduction before the E-MHSA module with point-wise convolutions to further accelerate inference. A shrinking ratio r is introduced for channel reduction. We also utilize Batch Normalization in the E-MHSA module for extremely efficient deployment.

Furthermore, NTB is equipped with an MHCA module that cooperates with the E-MHSA module to capture multi-frequency signals. After that, output features from E-MHSA and MHCA are concatenated to mix high-low-frequency information. Finally, an MLP layer is borrowed at the end to extract more essential and distinct features. Briefly, the implementation of NTB can be formulated as follows:

$$\begin{aligned} \dot{z}^l &= \text{Proj}(z^{l-1}) \\ \tilde{z}^l &= \text{E-MHSA}(\dot{z}^l) + \dot{z}^l \\ \bar{z}^l &= \text{Proj}(\tilde{z}^l) \\ \hat{z}^l &= \text{MHCA}(\bar{z}^l) + \bar{z}^l \\ \bar{z}^l &= \text{Concat}(\hat{z}^l, \tilde{z}^l) \\ z^l &= \text{MLP}(\bar{z}^l) + \bar{z}^l \end{aligned} \quad (6)$$

where \tilde{z}^l, \hat{z}^l and z^l denote the output of E-MHSA, MHCA and NTB, respectively. Proj denotes the point-wise convolution layer for channel projection. Also, NTB uniformly adopts BN and ReLU as the efficient norm and activation layers instead of LN and GELU. Compared with traditional

Table 1. Comparison of different hybrid strategies. Cls denotes ImageNet-1K classification task. Det denotes detection task on COCO dataset with Mask-RCNN $1 \times$. Seg denotes segmentation task with Semantic FPN 80k on ADE20K dataset. TensorRT latency is uniformly measured with the input size of $8 \times 3 \times 224 \times 224$.

Model	Latency(ms)	Cls	Det	Seg
	TensorRT	Acc(%)	AP ^b	mIoU(%)
ResNet101	7.8	80.8	40.4	38.8
C C C C	7.8	82.1	44.1	43.7
C C C T	7.8	82.4	44.7	45.6
C C T T	7.8	81.5	44.0	45.2
C T T T	8.0	80.6	42.6	44.7
C C C H _N	7.7	82.1	44.6	45.2
C C H _N H _N	7.7	82.3	45.2	46.3
C H_N H_N H_N	7.7	82.3	45.5	46.5
H _N H _N H _N H _N	7.8	81.7	44.5	45.9

Table 2. Comparison of different patterns in NHS and exploration of different hyper-parameters configurations. S1,S2,S3 and S4 denote Stage1, Stage2, Stage3 and Stage4 respectively.

Hybrid Strategy	Model	Configs				Latency(ms)	Cls	Det	Seg
		S1	S2	S3	S4	TensorRT	Acc(%)	AP ^b	mIoU(%)
$\begin{bmatrix} \text{NCB} \times \mathcal{N} \\ \text{NTB} \times 1 \end{bmatrix}$	Small	3	4	(11+1)	3	7.7	82.3	45.5	46.5
	Base	3	4	(22+1)	3	9.7	83.0	45.8	47.2
	Large	3	4	(33+1)	3	11.7	83.2	46.2	47.5
$\begin{bmatrix} \text{NCB} \times \mathcal{N} \\ \text{NTB} \times 1 \end{bmatrix} \times L$	Small	3	4	(1+1) \times 3	3	7.4	82.1	44.9	46.4
		3	4	(2+1) \times 3	3	8.0	82.5	45.6	46.4
		3	4	(3+1) \times 3	3	8.5	82.6	46.1	47.1
		3	4	(4+1)\times2	3	7.7	82.4	45.8	47.0
	3	4	(5+1) \times 2	3	8.1	82.5	45.8	47.1	
	Base Large	3	4	(4+1)\times4	3	10.5	83.3	47.2	48.8
		3	4	(4+1)\times6	3	13.0	83.6	48.0	50.4

Transformer block, NTB is capable of capturing and mixing multi-frequency information in the lightweight mechanism which greatly boosts model performance.

3.4. Next Hybrid Strategy (NHS)

Some recent works [4, 18, 24, 37] have paid great efforts to combine CNN and Transformer for efficient deployment. As shown in Figure 4(b)(c), almost all of them monotonously adopt convolution blocks in the shallow stages and just stack Transformer blocks in the last one or two stages which presents effective results in the classification task. Unfortunately, we observe that these traditional hybrid strategies are effortless to reach performance saturation on downstream tasks (e.g. segmentation and detection). The reason is, the classification task just uses outputs from the last stage for prediction while downstream tasks (e.g. segmentation and detection) usually rely on features from each stage to gain better results. The traditional hybrid strategies, however, just stack Transformer blocks in the last few stages. The shallow stages thus fail to capture global information, e.g. global shapes and structures of object, which is vital to segmentation and detection tasks.

To overcome the defeats of existing hybrid strategies, we propose a Next Hybrid Strategy (NHS) from a new

insight, which creatively stacks convolution block (NCB) and Transformer block (NTB) with $(N + 1) * L$ hybrid paradigm. NHS significantly promotes model performance in downstream tasks under controlling the proportion of Transformer block for efficient deployment. Firstly, in order to endow the shallow stages with the capability of capturing global information, we present a novel hybrid strategy in $(NCB \times N + NTB \times 1)$ pattern, which sequentially stack N NCB and one NTB in each stage as shown in Figure 4(d). Specifically, the Transformer block(NTB) is placed at the end of each stage, which enables the model to learn global representation in the shallow layers. We conduct a series of experiments to verify the superiority of the proposed hybrid strategy. The performances of difference hybrid strategies are shown in Table 1. C denotes uniformly stacking convolution block(NCB) in one stage and T denotes consistently building one stage with Transformer block(NTB). Specially, H_N indicates stacking NCB and NTB with $(NCB \times N + NTB \times 1)$ pattern in the corresponding stage. All models in Table 1 are equipped with four stages. For example, CCCC represents consistently using convolution block in all of the four stages. For fair comparison, we build all the model under similar TensorRT latency. More implementation details are presented in Section 4. As shown in Table 1, the proposed hybrid strategy significantly promotes model performance compared with existing methods in the downstream tasks. $C H_N H_N H_N$ achieve the best overall performance. For example, $C H_N H_N H_N$ surpass $C C C T$ 0.8 mAP in detection and 0.9% mIoU in segmentation. Besides, The results of $H_N H_N H_N H_N$ shows that placing Transformer block in the first stage will deteriorate the latency-accuracy trade-off of model.

We further verify the general effectiveness of $C H_N H_N H_N$ on large model by increasing the number of blocks in the third stage as ResNet [9]. Experimental results of the first three rows in Table 2 show that the performance of large model is hard to promote and gradually reaches saturation. Such a phenomenon indicates that expanding model size by enlarging the N of $(NCB \times N + NTB \times 1)$ pattern, i.e. simply adding more convolution block is not the best choice. It also implies that the value of N in $(NCB \times N + NTB \times 1)$ pattern may seriously affect the model performance. We thus begin to explore the impact of the value of N on the model performance through extensive experiments. As shown in Table 2 (middle), we build models with different configurations of N on the third stage. To build model with similar latency for fair comparison, we stack L groups of $(NCB \times N + NTB \times 1)$ pattern when the value of N is small. Surprisingly, we found that stack NCB and NTB in $(NCB \times N + NTB \times 1) \times L$ pattern achieve better model performance compared to $(NCB \times N + NTB \times 1)$ pattern.

Table 3. Detailed configurations of Next-ViT variants.

Stages	Output size	Layers	Next-ViT-S	Next-ViT-B	Next-ViT-L
Stem	$\frac{H}{4} \times \frac{W}{4}$	Convolution Layers	Conv $3 \times 3, C = 64, S = 2$		
			Conv $3 \times 3, C = 32, S = 1$		
			Conv $3 \times 3, C = 64, S = 1$		
			Conv $3 \times 3, C = 64, S = 2$		
Stage 1	$\frac{H}{4} \times \frac{W}{4}$	Patch Embedding	Conv $1 \times 1, C = 96$		
		Next-ViT Block	[NCB $\times 3$] $\times 1$		
Stage 2	$\frac{H}{8} \times \frac{W}{8}$	Patch Embedding	Avg.pool, $S = 2$		
		Next-ViT Block	Conv $1 \times 1, C = 192$		
Stage 3	$\frac{H}{16} \times \frac{W}{16}$	Patch Embedding	[NCB $\times 3$] $\times 1$		
		Next-ViT Block	Avg.pool, $S = 2$		
Stage 4	$\frac{H}{32} \times \frac{W}{32}$	Patch Embedding	Conv $1 \times 1, C = 384$		
		Next-ViT Block	[NCB $\times 4$] $\times 2$ [NCB $\times 4$] $\times 4$ [NCB $\times 4$] $\times 6$		
Stage 4	$\frac{H}{32} \times \frac{W}{32}$	Patch Embedding	Avg.pool, $S = 2$		
		Next-ViT Block	Conv $1 \times 1, C = 768$		
Stage 4	$\frac{H}{32} \times \frac{W}{32}$	Patch Embedding	[NCB $\times 2$] $\times 1$		
		Next-ViT Block	[NTB $\times 1$] $\times 1$		

It denotes that repeatedly combining low-frequency signal extractors and high-frequency signal extractors in a proper manner $((NCB \times N + NTB \times 1))$ leads to higher quality representation learning. As shown in Table 2, model with $N = 4$ in the third stage achieving the best trade-off between performance and latency. We further build the larger model by enlarging L of $(NCB \times 4 + NTB \times 1) \times L$ pattern in the third stage.

As shown in Table 2 (bottom), the performance of Base ($L = 4$) and Large ($L = 6$) model are significantly promote compared to small model, which verifies the general effectiveness of proposed $(NCB \times N + NTB \times 1) \times L$ pattern. We use $N = 4$ as the basic configurations in the rest of the paper.

We stack NCB and NTB with the above Next Hybrid Strategy to build Next-ViT, which can be formally defined as:

$$\text{Next-ViT}(X) = \oint_i \{[\Gamma(\Psi(X) \times N_i)] \times L_i\} \quad (7)$$

where $i \in (1, 2, 3, 4)$ denotes the stage index. Ψ means NCB. Γ means identity layer when $i = 1$, otherwise, NTB. Finally, \oint indicates the operation of stacking the stages sequentially.

3.5. Next-ViT Architectures

To provide a fair comparison with other SOTA networks, we present three typical variants, namely, Next-ViT-S/B/L. The architecture specifications are listed in Table 3, in which C represents the output channel of a stage and S denotes stride in convolution or Avg.pool. Additionally, the channel proportion ratio r of E-MHSA and MHCA in NTB is set as 0.75 and the spatial reduction ratio s in E-MHSA is [8, 4, 2, 1] in different stages. The expansion ratio of each MLP layer is set as 2, and the head dim in E-MHSA and

Table 4. Comparison of different state-of-the-art methods on ImageNet-1K classification task. (*)CMT use HardSwish which is not well supported by CoreML, we replace it with GELU for fair comparison.

Method	Image	Param	FLOPs	Latency(ms)		Top-1 (%)
	Size	(M)	(G)	TensorRT	CoreML	
ResNet101 [9]	224	44.6	7.9	7.8	4.0	80.8
ResNeXt101-32x4d [39]	224	44.2	8.0	8.0	4.0	78.8
RegNetY-8G [27]	224	44.2	8.0	11.4	4.1	81.7
ResNeSt50 [43]	224	27.5	5.4	102.7	36.6	81.1
EfficientNet-B3 [31]	300	12.0	1.8	12.5	5.8	81.5
MobileViTv2-1.0 [25]	256	4.9	4.9	-	2.9	78.1
MobileViTv2-2.0 [25]	256	18.5	7.5	-	6.7	81.2
ConvNeXt-T [21]	224	29.0	4.5	19.0	83.8	82.1
DeiT-T [32]	224	5.9	1.2	6.7	4.5	72.2
DeiT-S [32]	224	22.0	4.6	11.4	9.0	79.8
Swin-T [20]	224	29.0	4.5	-	-	81.3
PVTv2-B2 [34]	224	25.4	4.0	34.5	96.7	82.0
Twins-SVT-S [3]	224	24.0	2.9	17.3	-	81.7
PoolFormer-S24 [41]	224	21.1	3.4	14.4	6.2	80.3
PoolFormer-S36 [41]	224	31.2	5.0	21.8	6.7	81.4
CMT-T(*) [7]	160	9.5	0.6	11.8	4.6	79.1
CMT-XS(*) [7]	192	15.2	1.5	21.9	8.3	81.8
Coat Tiny [40]	224	5.5	4.4	52.9	55.4	78.3
CvT-13 [36]	224	20.1	4.5	18.1	62.6	81.6
Next-ViT-S	224	31.7	5.8	7.7	3.5	82.4
Next-ViT-S	384	31.7	17.3	21.6	8.9	83.6
ResNet152 [9]	224	60.2	4.0	11.3	5.0	81.7
ResNeXt101-64x4d [39]	224	83.5	15.6	13.6	6.8	79.6
ResNeSt101 [43]	224	48.0	10.2	149.8	45.4	83.0
ConvNeXt-S [21]	224	50.0	8.7	28.1	159.5	83.1
Swin-S [20]	224	50.0	8.7	-	-	83.0
PVTv2-B3 [34]	224	45.2	6.9	55.8	107.7	83.2
Twins-SVT-B [3]	224	56.0	8.6	32.0	-	83.2
PoolFormer-M36 [41]	224	56.1	8.8	28.2	-	82.1
CSWin-T [5]	224	23.0	4.3	29.5	-	82.7
Coat Mini [40]	224	10.0	6.8	68.0	60.8	81.0
CvT-21 [36]	224	32.0	7.1	28.0	91.4	82.1
UniFormer-S [17]	224	22.1	3.6	14.4	4.6	82.9
TRT-ViT-C [37]	224	67.3	5.9	9.2	5.0	82.7
EfficientFormer-L7 [18]	224	82.0	7.9	17.4	6.9	83.3
Next-ViT-B	224	44.8	8.3	10.5	4.5	83.3
Next-ViT-B	384	44.8	24.6	29.6	12.4	84.4
RegNetY-16G [27]	224	84.0	16.0	18.0	7.4	82.9
EfficientNet-B5 [31]	456	30.0	9.9	64.4	23.2	83.7
ConvNeXt-B [21]	224	88.0	15.4	37.3	247.6	83.9
DeiT-B [32]	224	87.0	17.5	31.0	18.2	81.8
Swin-B [20]	224	88.0	15.4	-	-	83.3
PVTv2-B4 [34]	224	62.6	10.1	70.8	139.8	83.6
Twins-SVT-L [3]	224	99.2	15.1	44.1	-	83.7
PoolFormer-M48 [41]	224	73.2	11.6	38.2	-	82.5
CSWin-S [5]	224	35.0	6.9	45.0	-	83.6
CMT-S(*) [7]	224	25.1	4.0	52.0	14.6	83.5
Coat Small [40]	224	22.0	12.6	82.7	122.4	82.1
UniFormer-B [17]	224	50.2	8.3	31.0	9.0	83.9
TRT-ViT-D [37]	224	103.0	9.7	15.1	8.3	83.4
Next-ViT-L	224	57.8	10.8	13.0	5.5	83.6
Next-ViT-L	384	57.8	10.8	36.0	15.2	84.6

MHCA is set as 32. For normalization and activation functions, both NCB and NTB blocks use BatchNorm [14] and ReLU.

4. Experimental Results

4.1. ImageNet-1K Classification

4.1.1 Implementation

We carry out the image classification experiment on the ImageNet-1K [28], which contains about 1.28M training

images and 50K validation images from 1K categories. For a fair comparison, we follow the training settings of the recent vision Transformer [3, 35] with minor changes. Concretely, all of the Next-ViT variants are trained for 300 epochs on 8 V100 GPUs with a total batch size of 2048. The resolution of the input image is resized to 224×224 . We adopt the AdamW [22] as the optimizer with weight decay 0.1. The learning rate is gradually decayed based on the cosine strategy with the initialization of $2e-3$ and the use of a linear warm-up strategy with 20 epochs for all Next-ViT variants. Besides, we have also employed the increasing stochastic depth augmentation [13] with the maximum drop-path rate of 0.1, 0.2, 0.2 for Next-ViT-S/B/L. With the input size corresponding to the respective method, latency in Table 4 is uniformly measured based on the TensorRT-8.0.3 framework with a T4 GPU (batch size=8) and CoreML framework on an iPhone12 Pro Max with iOS 16.0 (batch size=1). Note that both the iPhone 12 and iPhone 12 Pro Max are equipped with the same A14 processor.

4.1.2 Comparison with State-of-the-art Models

As shown in Table 4, compared to the latest state-of-the-art methods (e.g. CNNs, ViTs and hybrid networks), we achieve the best trade-off between accuracy and latency. Specifically, compared with the famous CNNs such as ResNet101 [9], Next-ViT-S improve the accuracy by 1.6% with a similar latency on TensorRT and faster speed on CoreML (from 4.0ms to 3.5ms). Meanwhile, Next-ViT-L achieves the similar accuracy as EfficientNet-B5 [31] and ConvNeXt-B while $4.0\times$ and $1.4\times$ faster on TensorRT, $3.2\times$ and $44\times$ faster on CoreML. In terms of the advanced ViTs, Next-ViT-S outperforms Twins-SVT-S [3] by 0.7% with $1.3\times$ faster inference speed on TensorRT. Next-ViT-B surpass CSwin-T [5] by 0.6% while the inference latency is compressed by 64% on TensorRT. Finally, compared with recent hybrid methods, Next-ViT-S beats CMT-XS by 0.6% with $1.8\times$ and $1.4\times$ faster speed on TensorRT and CoreML. Compared to EfficientFormer-L7 [18], Next-ViT-B predict with 35% fewer runtime on CoreML and 40% fewer runtime on TensorRT while the performance is similar. Next-ViT-L also obtains a 15% inference latency gain and achieves a better performance than TRT-ViT-D. These results demonstrate that the proposed Next-ViT design is an effective and promising paradigm.

4.2. ADE20K Semantic Segmentation

4.2.1 Implementation

To further verify the capacity of our Next-ViT, we conduct the semantic segmentation experiment on ADE20K [45], which contains about 20K training images and 2K validation images from 150 categories. To make fair comparisons,

Table 5. Comparison of different backbones on ADE20K semantic segmentation task. FLOPs are measured with the input size of 512×2048 .

Backbone	Latency(ms)		Semantic FPN 80k			UperNet 160k		
	TensorRT	CoreML	Param(M)	FLOPs(G)	mIoU(%)	Param(M)	FLOPs(G)	mIoU/MS mIoU(%)
ResNet101 [9]	32.8	13.2	48.0	260	38.8	96	1029	-/44.9
ResNeXt101-32x4d [39]	37.0	15.3	47.1	-	39.7	-	-	-/-
ResNeSt50(*) [43]	522.3	372.3	30.4	204	39.7	68.4	973	42.1/-
ConvNeXt-T [21]	78.5	349.4	-	-	-	60.0	939	-/46.7
Swin-T [20]	-	-	31.9	182	41.5	59.9	945	44.5/45.8
PVTv2-B2 [34]	167.6	101.0	29.1	-	45.2	-	-	-/-
Twins-SVT-S [3]	127.2	-	28.3	144	43.2	54.4	901	46.2/47.1
PoolFormer-S12 [41]	30.3	18.2	15.7	-	37.2	-	-	-/-
PoolFormer-S24 [41]	59.1	23.0	23.2	-	40.3	-	-	-/-
TRT-ViT-C [37]	40.6	20.7	70.6	213	46.2	105.0	978	47.6/48.9
EfficientFormer-L3 [18]	35.9	10.6	-	-	43.5	-	-	-/-
Next-ViT-S	38.2	18.1	36.2	207	47.0	66.3	968	48.3/49.0
ResNeXt101-64x4d [39]	65.7	25.6	86.4	-	40.2	-	-	-/-
ResNeSt101(*) [43]	798.9	443.6	51.2	305	42.4	89.2	1074	44.2/-
ConvNeXt-S [21]	131.5	658.0	-	-	-	82.0	1027	-/49.6
Swin-S [20]	-	-	53.2	274	45.2	81.3	1038	47.6/49.5
PVTv2-B3 [34]	230.9	114.5	49.0	-	47.3	-	-	-/-
Twins-SVT-B [3]	231.8	-	60.4	261	45.3	88.5	1020	47.7/48.9
PoolFormer-S36 [41]	87.7	27.7	34.6	-	42.0	-	-	-/-
PoolFormer-M36 [41]	127.8	32.0	59.8	-	42.4	-	-	-/-
CSWin-T [5]	182.3	-	26.1	202	48.2	59.9	959	49.3/50.4
UniFormer-S [17]	90.7	33.5	25.0	247	46.6	52.0	1088	47.6/48.5
TRT-ViT-D [37]	58.1	29.4	105.9	296	46.7	143.7	1065	48.8/49.8
EfficientFormer-L7 [18]	84.0	23.0	-	-	45.1	-	-	-/-
Next-ViT-B	51.6	24.4	49.3	259	48.7	79.3	1019	49.3/49.9
ConvNeXt-B [21]	181.3	1074.4	-	-	-	122.0	1170	-/49.9
Swin-B [20]	-	-	91.2	422	46.0	121.0	1188	48.1/49.7
PVTv2-B4 [34]	326.4	147.6	66.3	-	47.9	-	-	-/-
Twins-SVT-L [3]	409.7	-	103.7	404	46.7	133.0	1164	48.8/49.7
PoolFormer-M48 [41]	168.7	39.5	77.1	-	42.7	-	-	-/-
CSWin-S [5]	298.2	-	38.5	271	49.2	64.4	1027	50.4/51.5
UniFormer-B [17]	195.1	70.6	54.0	471	48.0	80.0	1227	50.0/50.8
Next-ViT-L	65.3	30.1	62.3	331	49.0	92.3	1071	50.4/51.1

we also follow the training conventions of the previous vision Transformers [3, 20, 35] on the Semantic FPN [16] and UperNet [38] frameworks. All of our models are pre-trained on the ImageNet-1k and then finetuned on ADE20K with the input size of 512×512 . For the Semantic FPN framework, we adopt the AdamW optimizer with both the learning rate and weight decay being 0.0001. Then we train the whole network for 80K iterations with a total batch size of 16 based on the stochastic depth of 0.2 for Next-ViT-S/B/L. For the training and testing on the UperNet framework, we also train the models for 160K iterations with the stochastic depth of 0.2. AdamW optimizer is used as well but with the learning rate 6×10^{-5} , total batch size 16, and weight decay 0.01. Then we test the mIoU based on both single-scale and multi-scale (MS) where the scale goes from 0.5 to 1.75 with an interval of 0.25. For detection and segmentation tasks, due to some modules in Mask R-CNN and Upernet

are not easy to be deployed on TensorRT and CoreML, we only measure the latency of the backbone for a fair comparison, with the same test environments as classification. For simplicity, the input size of 512×512 is uniformly used to measure latency in Table 5 and Table 6.

4.2.2 Comparison with State-of-the-art Models

In Table 5, we make a comparison with CNNs, ViTs, and recent hybrid methods as well. Next-ViT-S surpasses ResNet101 [9] and ResNeXt101-32x4d [39] by 8.2% and 7.3% mIoU, respectively. Next-ViT-B beats CSwin-T by 0.5% mIoU and the inference speed is accelerated by $2.5 \times$ on TensorRT. Compared with the UniFormer-S/B [17], Next-ViT-B/L achieves 2.1% and 1.0% mIoU performance gain while $0.4 \times / 1.3 \times$ faster on CoreML and $0.8 \times / 1.6 \times$ faster on TensorRT. Next-ViT-B surpass EfficientFormer-L7

Table 6. Comparison of different backbones on Mask R-CNN-based object detection and instance segmentation tasks. FLOPs are measured with the input size of 800×1280 . The superscript b and m denote the box detection and mask instance segmentation.

Backbone	Param (M)	FLOPs (G)	Latency(ms)		Mask R-CNN 1×					Mask R-CNN 3× + MS						
			TensorRT	CoreML	AP ^b	AP ₅₀ ^b	AP ₇₅ ^b	AP ^m	AP ₅₀ ^m	AP ₇₅ ^m	AP ^b	AP ₅₀ ^b	AP ₇₅ ^b	AP ^m	AP ₅₀ ^m	AP ₇₅ ^m
ResNet101 [9]	63.2	336	32.8	13.2	40.4	61.1	44.2	36.4	57.7	38.8	42.8	63.2	47.1	38.5	60.1	41.3
ResNeXt101-32x4d [39]	62.8	-	37.0	15.3	41.9	62.5	45.9	37.5	59.4	40.2	-	-	-	-	-	-
ResNeSt50(*) [43]	47.4	400	522.3	372.3	42.6	-	-	38.1	-	-	-	-	-	-	-	-
ConvNext-T [21]	-	262	78.5	349.4	-	-	-	-	-	-	46.2	67.9	50.8	41.7	65.0	44.9
Swin-T [20]	47.8	264	-	-	42.2	64.4	46.2	39.1	64.6	42.0	46.0	68.2	50.2	41.6	65.1	44.8
PVTv2-B2 [34]	45.0	-	167.6	101.0	45.3	67.1	49.6	41.2	64.2	44.4	-	-	-	-	-	-
Twins-SVT-S [3]	44.0	228	127.2	-	43.4	66.0	47.3	40.3	63.2	43.4	46.8	69.2	51.2	42.6	66.3	45.8
PoolFormer-S12 [41]	31.6	-	30.3	18.2	37.3	59.0	40.1	34.6	55.8	36.9	-	-	-	-	-	-
PoolFormer-S24 [41]	41.0	-	59.1	22.9	40.1	62.2	43.4	37.0	59.1	39.6	-	-	-	-	-	-
TRT-ViT-C [37]	86.3	294	40.6	20.8	44.7	66.9	48.8	40.8	63.9	44.0	47.3	68.8	51.9	42.7	65.9	46.0
EfficientFormer-L3 [18]	-	-	35.9	10.6	41.4	63.9	44.7	38.1	61.0	40.4	-	-	-	-	-	-
Next-ViT-S	38.2	289	38.2	18.1	45.8	68.2	50.3	41.7	65.3	44.6	48.1	70.0	52.8	43.2	66.8	46.7
ResNeXt101-64x4d [39]	101.9	-	65.7	25.6	42.8	63.8	47.3	38.4	60.6	41.3	-	-	-	-	-	-
ResNeSt101(*) [43]	68.1	499	798.9	443.6	45.2	-	-	40.2	-	-	-	-	-	-	-	-
Swin-S [20]	69.1	354	-	-	44.8	66.6	48.9	40.9	63.4	44.2	48.5	70.2	53.5	43.3	67.3	46.6
PVTv2-B3 [34]	64.9	-	230.9	114.5	47.0	68.1	51.7	42.5	65.7	45.7	-	-	-	-	-	-
Twins-SVT-B [3]	76.3	340	231.8	-	45.2	67.6	49.3	41.5	64.5	44.8	48.0	69.5	52.7	43.0	66.8	46.6
CSWin-T [5]	42.0	279	182.3	-	46.7	68.6	51.3	42.2	65.6	45.4	49.0	70.7	53.7	43.6	67.9	46.6
PoolFormer-S36 [41]	50.5	-	87.7	27.7	41.0	63.1	44.8	37.7	60.1	40.0	-	-	-	-	-	-
CMT-S [5]	30.2	-	200.5	73.4	44.6	66.8	48.9	40.7	63.9	43.4	-	-	-	-	-	-
CoaT Mini [40]	41.6	-	509.6	476.9	45.1	-	-	40.6	-	-	46.5	-	-	41.8	-	-
UniFormer-S _{h14} [17]	41	269	164.0	-	45.6	68.1	49.7	41.6	64.8	45.0	48.2	70.4	52.5	43.4	67.1	47.0
TRT-ViT-D [37]	121.5	375	58.1	29.5	45.3	67.9	49.6	41.6	64.7	44.8	48.1	69.3	52.7	43.4	66.7	46.8
EfficientFormer-L7 [18]	-	-	84.0	23.0	42.6	65.1	46.1	39.0	62.2	41.7	-	-	-	-	-	-
Next-ViT-B	64.8	340	51.6	24.4	47.2	69.3	52.0	42.8	66.3	46.2	49.4	71.0	54.2	44.4	68.3	47.8
Swin-B [20]	107	496	-	-	46.9	-	-	42.3	-	-	48.5	69.8	53.2	43.4	66.8	46.9
PVTv2-B4 [34]	82.2	-	326.4	147.6	47.5	68.7	52.0	42.7	66.1	46.1	-	-	-	-	-	-
Twins-SVT-L [3]	111	474	409.7	-	45.7	-	-	41.6	-	-	-	-	-	-	-	-
CSWin-S [5]	54.0	342	298.2	-	47.9	70.1	52.6	43.2	67.1	46.2	50.0	71.3	54.7	44.5	68.4	47.7
CoaT Small [40]	54.0	-	601.7	612.9	46.5	-	-	41.8	-	-	49.0	-	-	43.7	-	-
UniFormer-B _{h14} [17]	69	399	367.7	-	47.4	69.7	52.1	43.1	66.0	46.5	50.3	72.7	55.3	44.8	69.0	48.3
Next-ViT-L	77.9	390	65.3	30.1	48.0	70.0	52.9	43.3	67.0	46.8	50.0	71.4	54.8	44.8	68.6	48.3

[18] by 3.6% mIoU with similar CoreML runtime and 38% fewer latency on TensorRT. In terms of the UperNet [38] framework, Next-ViT-S surpass recent SOTA CNN model ConvNeXt [21] 2.3% MS mIoU while 1.0× and 18.0× faster on TensorRT and CoreML respectively. Compared to the CSWin-S [5], Next-ViT-L achieves 3.6× faster speed on TensorRT with similar performance. Extensive experiments reveal that our Next-ViT achieves excellent potential on segmentation tasks.

4.3. Object Detection and Instance Segmentation

4.3.1 Implementation

Next, we evaluate Next-ViT on the objection detection and instance segmentation task [19] based on the Mask R-CNN [8] frameworks with COCO2017 [19]. Specifically, all of our models are pre-trained on ImageNet-1K and then finetuned following the settings of the previous works [3, 20, 35]. As for the 12 epochs (1×) experiment, we use the AdamW optimizer with the weight decay of 0.05. There are 500 iterations for a warm-up during the training, and the learning rate will decline by 10× at epochs 8 and 11. Based on the 36 epochs (3×) experiment with multi-

scale (MS) training, models are trained with the resized images such that the shorter side ranges from 480 to 800 and the longer side is at most 1333. The learning rate will decline by 10× at epochs 27 and 33. The other settings are the same as 1×.

4.3.2 Comparison with State-of-the-art Models

Table 6 shows the evaluation results with the Mask R-CNN framework. Based on the 1× schedule, Next-ViT-S surpass ResNet101 [9] and ResNeSt50 [43] by 5.4 AP^b and 3.2AP^b. Next-ViT-L beats PVTv2-B4 [34] by 0.5 AP^b and predict with 4.0× and 3.9× faster runtime on TensorRT and CoreML. Compared to the EfficientFormer-L7 [18], Next-ViT-B improves AP^b from 42.6 to 47.2 with similar CoreML latency and 39% fewer TensorRT runtime. Next-ViT-B outperforms TRT-ViT-D [37] by 1.9 AP^b but is still faster on both TensorRT and CoreML. Based on the 3× schedule, Next-ViT shows the same superiority as the 1×. Specifically, Next-ViT-S surpass ResNeXt101-32x4d by 5.3AP^b with similar latency. Compared to the Twins-SVT-S, Next-ViT-S achieves 1.3 AP^b higher performance but with 3.2× faster speed on TensorRT. Next-ViT-B out-

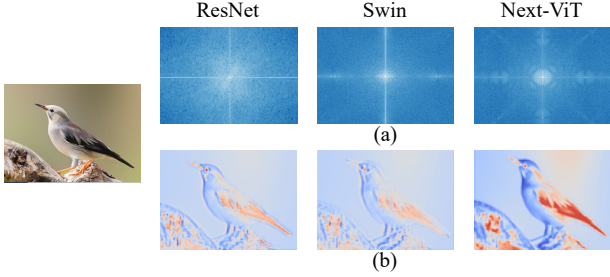


Figure 5. (a) Fourier spectrum of ResNet [9], Swin [20] and Next-ViT. (b) Heat maps of the output feature from ResNet [9], Swin [20] and Next-ViT.

performs CSwin-T by 0.4 AP^b but with 2.5× fewer prediction time. For the Next-ViT-L, it exhibits a similar performance on object detection and instance segmentation as CSwin [5] but the inference speed is accelerated by 79%.

4.4. Ablation Study and Visualization

To understand our Next-ViT better, we ablate each critical design by evaluating its performance on ImageNet-1K classification and downstream tasks. We also visualize the Fourier spectrum and Heat map of output features to show the intrinsic superiority of Next-ViT.

4.4.1 Impact of Next Convolution Block

To verify the effectiveness of the proposed NCB, we replace NCB in Next-ViT with famous blocks, such as Bottleneck in ResNet [9], ConvNeXt [21] block, LSA block in Twins [3], and etc. For a fair comparison, we consistently use NTB and NHS to build different models under similar latency on TensorRT.

As shown in Table 7, NCB achieves the best latency/accuracy trade-off on all of the three tasks, which verifies the advantage of the proposed NCB. For example, NCB outperforms the recent ConvNeXt block [9] by 2.8% in classification, 4.4 AP^b in detection and 2.9% mIoU in segmentation.

4.4.2 Impact of different ratio

Furthermore, we explore the effect of shrink ratio r of Next Transformer Block on the overall performance of Next-ViT. As stated in Table 8, decreasing the shrinking ratio r , i.e. the number of channels in E-MHSA module, will reduce the model latency. Furthermore, model with $r = 0.75$ and $r = 0.5$ achieve better performance over model with pure Transformer ($r = 1$). This denotes that fusing multi-frequency signals in a proper manner will enhance the model ability of representation learning.

Specially, model with $r = 0.75$ achieve the best latency/accuracy trade-off. It outperforms baseline model

Table 7. Comparison of different convolution blocks.

Block type	Latency(ms)	Cls	Det	Seg
	TensorRT	Acc(%)	AP ^b	mIoU(%)
Bottleneck Block [9]	7.8	81.9	44.5	46.1
ConvNeXt Block [21]	7.8	79.6	41.4	44.1
LSA Block [3]	8.4	78.2	38.7	40.3
PoolFormer Block [41]	7.6	80.9	42.3	44.3
Local MHRA Block [17]	7.8	80.5	42.4	43.8
NCB (ours)	7.7	82.4	45.8	47.0

Table 8. Comparison of results of different ratios.

r	Latency(ms)	Cls	Det	Seg
	TensorRT	Acc(%)	AP ^b	mIoU(%)
0.0	6.6	80.9	43.1	42.7
0.25	6.9	81.3	45.0	45.6
0.50	7.3	82.2	45.4	46.4
0.75	7.7	82.4	45.8	47.0
1.0	8.2	82.1	45.4	45.8

Table 9. Different normalizations and activations comparison.

Norm	Activation	Latency(ms)	Cls	Det	Seg
		TensorRT	Acc(%)	AP ^b	mIoU(%)
LN	GELU	9.3	82.7	46.0	47.3
LN	ReLU	9.1	82.7	46.0	47.2
BN	GELU	8.0	82.5	45.9	47.1
BN	ReLU	7.7	82.4	45.8	47.0

($r = 1.0$) with 0.3%, 0.3 AP^b and 1.2% mIoU on classification, detection and segmentation while is more lightweight. The above results indicate the effectiveness of the proposed NTB block.

4.4.3 Impact of Normalization and Activation

We further study the impact of different normalization layers and activation functions in Next-ViT. As shown in Table 9, both the LN and GELU bring negligible performance improvement but with significantly higher inference latency on TensorRT. On the other hand, BN and ReLU achieve the best latency/accuracy trade-off on overall tasks. Therefore, we uniformly use BN and ReLU in Next-ViT for efficient deployment in realistic industrial scenarios.

4.4.4 Visualization

To verify the superiority of our Next-ViT, we visualize the Fourier spectrum and heat maps of the output features from ResNet, Swin Transformer and Next-ViT in Figure 5 (a). The spectrum distribution of ResNet denotes that convolution blocks tend to capture high-frequency signals while difficult to focus on low-frequency information. On the other hand, ViT experts in capturing low-frequency signals

but ignore high-frequency signals. Finally, Next-ViT is capable of simultaneously capturing high-quality and multi-frequency signals, which shows the effectiveness of NTB.

Furthermore, As shown in Figure 5 (b), we can see that Next-ViT can capture richer texture information and more accurate global information (e.g. edge shape) compared with ResNet and Swin, which shows the stronger modeling capability of Next-ViT.

5. Conclusion

In this paper, we present a family of Next-ViT that stacks efficient Next Convolution Block and Next Transformer Block in a novel strategy to build powerful CNN-Transformer hybrid architecture for efficient deployment on both mobile device and server GPU. Experimental results demonstrate that Next-ViT achieves a state-of-the-art latency/accuracy trade-off across diverse visual tasks, such as image classification, object detection and semantic segmentation. We hope that our work will provide new insights and promote more research in neural network architecture design for realistic industrial deployment.

References

- [1] Jean Bullier. Integrated model of visual processing. *Brain research reviews*, 36(2-3):96–107, 2001. [5](#)
- [2] Yinpeng Chen, Xiyang Dai, Dongdong Chen, Mengchen Liu, Xiaoyi Dong, Lu Yuan, and Zicheng Liu. Mobileformer: Bridging mobilenet and transformer. *arXiv preprint arXiv:2108.05895*, 2021. [4](#)
- [3] Xiangxiang Chu, Zhi Tian, Yuqing Wang, Bo Zhang, Haibing Ren, Xiaolin Wei, Huaxia Xia, and Chunhua Shen. Twins: Revisiting the design of spatial attention in vision transformers. *arXiv preprint arXiv:2104.13840*, 2021. [8](#), [9](#), [10](#), [11](#)
- [4] Zihang Dai, Hanxiao Liu, Quoc V Le, and Mingxing Tan. Coatnet: Marrying convolution and attention for all data sizes. *Advances in Neural Information Processing Systems*, 34:3965–3977, 2021. [1](#), [6](#)
- [5] Xiaoyi Dong, Jianmin Bao, Dongdong Chen, Weiming Zhang, Nenghai Yu, Lu Yuan, Dong Chen, and Baining Guo. Cswin transformer: A general vision transformer backbone with cross-shaped windows. *arXiv preprint arXiv:2107.00652*, 2021. [5](#), [8](#), [9](#), [10](#), [11](#)
- [6] Alexey Dosovitskiy, Lucas Beyer, Alexander Kolesnikov, Dirk Weissenborn, Xiaohua Zhai, Thomas Unterthiner, Mostafa Dehghani, Matthias Minderer, Georg Heigold, Sylvain Gelly, et al. An image is worth 16x16 words: Transformers for image recognition at scale. *arXiv preprint arXiv:2010.11929*, 2020. [4](#)
- [7] Jianyuan Guo, Kai Han, Han Wu, Chang Xu, Yehui Tang, Chunjing Xu, and Yunhe Wang. Cmt: Convolutional neural networks meet vision transformers. *arXiv preprint arXiv:2107.06263*, 2021. [4](#), [8](#)
- [8] Kaiming He, Georgia Gkioxari, Piotr Dollár, and Ross Girshick. Mask r-cnn. In *Proceedings of the IEEE International Conference on Computer Vision*, pages 2961–2969, 2017. [10](#)
- [9] Kaiming He, Xiangyu Zhang, Shaoqing Ren, and Jian Sun. Deep residual learning for image recognition. In *Proceedings of the IEEE Conference on Computer Vision and Pattern Recognition*, pages 770–778, 2016. [3](#), [4](#), [7](#), [8](#), [9](#), [10](#), [11](#)
- [10] Byeongho Heo, Sangdoon Yun, Dongyoon Han, Sanghyuk Chun, Junsuk Choe, and Seong Joon Oh. Rethinking spatial dimensions of vision transformers. In *Proceedings of the IEEE/CVF International Conference on Computer Vision*, pages 11936–11945, 2021. [4](#)
- [11] Andrew G Howard, Menglong Zhu, Bo Chen, Dmitry Kalenichenko, Weijun Wang, Tobias Weyand, Marco Andreetto, and Hartwig Adam. Mobilenets: Efficient convolutional neural networks for mobile vision applications. *arXiv preprint arXiv:1704.04861*, 2017. [3](#)
- [12] Gao Huang, Zhuang Liu, Laurens Van Der Maaten, and Kilian Q Weinberger. Densely connected convolutional networks. In *Proceedings of the IEEE conference on computer vision and pattern recognition*, pages 4700–4708, 2017. [3](#)
- [13] Gao Huang, Yu Sun, Zhuang Liu, Daniel Sedra, and Kilian Q Weinberger. Deep networks with stochastic depth. In *European Conference on Computer Vision*, pages 646–661, 2016. [8](#)
- [14] Sergey Ioffe and Christian Szegedy. Batch normalization: Accelerating deep network training by reducing internal covariate shift. In *International conference on machine learning*, pages 448–456. PMLR, 2015. [8](#)
- [15] Louise Kauffmann, Stephen Ramanoël, and Carole Peyrin. The neural bases of spatial frequency processing during scene perception. *Frontiers in integrative neuroscience*, 8:37, 2014. [5](#)
- [16] Alexander Kirillov, Ross Girshick, Kaiming He, and Piotr Dollár. Panoptic feature pyramid networks. In *Proceedings of the IEEE/CVF Conference on Computer Vision and Pattern Recognition*, pages 6399–6408, 2019. [9](#)
- [17] Kunchang Li, Yali Wang, Junhao Zhang, Peng Gao, Guanglu Song, Yu Liu, Hongsheng Li, and Yu Qiao. Uniformer: Unifying convolution and self-attention for visual recognition. *arXiv preprint arXiv:2201.09450*, 2022. [4](#), [8](#), [9](#), [10](#), [11](#)
- [18] Yanyu Li, Geng Yuan, Yang Wen, Eric Hu, Georgios Evangelidis, Sergey Tulyakov, Yanzhi Wang, and Jian Ren. Efficientformer: Vision transformers at mobilenet speed. *arXiv preprint arXiv:2206.01191*, 2022. [1](#), [4](#), [6](#), [8](#), [9](#), [10](#)
- [19] Tsung-Yi Lin, Michael Maire, Serge Belongie, James Hays, Pietro Perona, Deva Ramanan, Piotr Dollár, and C Lawrence Zitnick. Microsoft coco: Common objects in context. In *European Conference on Computer Vision*, pages 740–755, 2014. [10](#)
- [20] Ze Liu, Yutong Lin, Yue Cao, Han Hu, Yixuan Wei, Zheng Zhang, Stephen Lin, and Baining Guo. Swin transformer: Hierarchical vision transformer using shifted windows. *arXiv preprint arXiv:2103.14030*, 2021. [1](#), [4](#), [5](#), [8](#), [9](#), [10](#), [11](#)
- [21] Zhuang Liu, Hanzi Mao, Chao-Yuan Wu, Christoph Feichtenhofer, Trevor Darrell, and Saining Xie. A convnet for the

- 2020s. *arXiv preprint arXiv:2201.03545*, 2022. [3](#), [4](#), [5](#), [8](#), [9](#), [10](#), [11](#)
- [22] Ilya Loshchilov and Frank Hutter. Decoupled weight decay regularization. *arXiv preprint arXiv:1711.05101*, 2017. [8](#)
- [23] Ningning Ma, Xiangyu Zhang, Hai-Tao Zheng, and Jian Sun. Shufflenet v2: Practical guidelines for efficient cnn architecture design. In *Proceedings of the European Conference on Computer Vision*, pages 116–131, 2018. [3](#)
- [24] Sachin Mehta and Mohammad Rastegari. Mobilevit: light-weight, general-purpose, and mobile-friendly vision transformer. *arXiv preprint arXiv:2110.02178*, 2021. [1](#), [4](#), [6](#)
- [25] Sachin Mehta and Mohammad Rastegari. Separable self-attention for mobile vision transformers. *arXiv preprint arXiv:2206.02680*, 2022. [8](#)
- [26] Namuk Park and Songkuk Kim. How do vision transformers work? *arXiv preprint arXiv:2202.06709*, 2022. [5](#)
- [27] Ilija Radosavovic, Raj Prateek Kosaraju, Ross Girshick, Kaiming He, and Piotr Dollár. Designing network design spaces. In *Proceedings of the IEEE/CVF Conference on Computer Vision and Pattern Recognition*, pages 10428–10436, 2020. [8](#)
- [28] Olga Russakovsky, Jia Deng, Hao Su, Jonathan Krause, Sanjeev Satheesh, Sean Ma, Zhiheng Huang, Andrej Karpathy, Aditya Khosla, Michael Bernstein, et al. Imagenet large scale visual recognition challenge. *International Journal of Computer Vision*, 115(3):211–252, 2015. [8](#)
- [29] Mark Sandler, Andrew Howard, Menglong Zhu, Andrey Zhmoginov, and Liang-Chieh Chen. Mobilenetv2: Inverted residuals and linear bottlenecks. In *Proceedings of the IEEE Conference on Computer Vision and Pattern Recognition*, pages 4510–4520, 2018. [3](#)
- [30] Aravind Srinivas, Tsung-Yi Lin, Niki Parmar, Jonathon Shlens, Pieter Abbeel, and Ashish Vaswani. Bottleneck transformers for visual recognition. In *Proceedings of the IEEE/CVF conference on computer vision and pattern recognition*, pages 16519–16529, 2021. [4](#)
- [31] Mingxing Tan and Quoc Le. Efficientnet: Rethinking model scaling for convolutional neural networks. In *International Conference on Machine Learning*, pages 6105–6114, 2019. [8](#)
- [32] Hugo Touvron, Matthieu Cord, Matthijs Douze, Francisco Massa, Alexandre Sablayrolles, and Hervé Jégou. Training data-efficient image transformers & distillation through attention. In *International Conference on Machine Learning*, pages 10347–10357, 2021. [4](#), [8](#)
- [33] Ashish Vaswani, Noam Shazeer, Niki Parmar, Jakob Uszkoreit, Llion Jones, Aidan N Gomez, Łukasz Kaiser, and Illia Polosukhin. Attention is all you need. *Advances in neural information processing systems*, 30, 2017. [5](#)
- [34] Wenhai Wang, Enze Xie, Xiang Li, Deng-Ping Fan, Kaitao Song, Ding Liang, Tong Lu, Ping Luo, and Ling Shao. Pvtv2: Improved baselines with pyramid vision transformer. *arXiv preprint arXiv:2106.13797*, 2021. [6](#), [8](#), [9](#), [10](#)
- [35] Wenhai Wang, Enze Xie, Xiang Li, Deng-Ping Fan, Kaitao Song, Ding Liang, Tong Lu, Ping Luo, and Ling Shao. Pyramid vision transformer: A versatile backbone for dense prediction without convolutions. *arXiv preprint arXiv:2102.12122*, 2021. [1](#), [8](#), [9](#), [10](#)
- [36] Haiping Wu, Bin Xiao, Noel Codella, Mengchen Liu, Xiyang Dai, Lu Yuan, and Lei Zhang. Cvt: Introducing convolutions to vision transformers. In *Proceedings of the IEEE/CVF International Conference on Computer Vision*, pages 22–31, 2021. [4](#), [8](#)
- [37] Xin Xia, Jiashi Li, Jie Wu, Xing Wang, Mingkai Wang, Xuefeng Xiao, Min Zheng, and Rui Wang. Trt-vit: Tensorrt-oriented vision transformer. *arXiv preprint arXiv:2205.09579*, 2022. [6](#), [8](#), [9](#), [10](#)
- [38] Tete Xiao, Yingcheng Liu, Bolei Zhou, Yuning Jiang, and Jian Sun. Unified perceptual parsing for scene understanding. In *European Conference on Computer Vision*, pages 418–434, 2018. [9](#), [10](#)
- [39] Saining Xie, Ross Girshick, Piotr Dollár, Zhuowen Tu, and Kaiming He. Aggregated residual transformations for deep neural networks. In *Proceedings of the IEEE Conference on Computer Vision and Pattern Recognition*, pages 1492–1500, 2017. [8](#), [9](#), [10](#)
- [40] Weijian Xu, Yifan Xu, Tyler Chang, and Zhuowen Tu. Co-scale conv-attentional image transformers. In *Proceedings of the IEEE/CVF International Conference on Computer Vision*, pages 9981–9990, 2021. [8](#), [10](#)
- [41] Weihao Yu, Mi Luo, Pan Zhou, Chenyang Si, Yichen Zhou, Xinchao Wang, Jiashi Feng, and Shuicheng Yan. Metaformer is actually what you need for vision. In *Proceedings of the IEEE/CVF Conference on Computer Vision and Pattern Recognition*, pages 10819–10829, 2022. [4](#), [5](#), [8](#), [9](#), [10](#), [11](#)
- [42] Li Yuan, Yunpeng Chen, Tao Wang, Weihao Yu, Yujun Shi, Zi-Hang Jiang, Francis EH Tay, Jiashi Feng, and Shuicheng Yan. Tokens-to-token vit: Training vision transformers from scratch on imagenet. In *Proceedings of the IEEE/CVF International Conference on Computer Vision*, pages 558–567, 2021. [4](#)
- [43] Hang Zhang, Chongruo Wu, Zhongyue Zhang, Yi Zhu, Haibin Lin, Zhi Zhang, Yue Sun, Tong He, Jonas Mueller, R Manmatha, et al. Resnest: Split-attention networks. In *Proceedings of the IEEE/CVF Conference on Computer Vision and Pattern Recognition*, pages 2736–2746, 2022. [8](#), [9](#), [10](#)
- [44] Xiangyu Zhang, Xinyu Zhou, Mengxiao Lin, and Jian Sun. Shufflenet: An extremely efficient convolutional neural network for mobile devices. In *Proceedings of the IEEE Conference on Computer Vision and Pattern Recognition*, pages 6848–6856, 2018. [3](#)
- [45] Bolei Zhou, Hang Zhao, Xavier Puig, Sanja Fidler, Adela Barriuso, and Antonio Torralba. Scene parsing through ade20k dataset. In *Proceedings of the IEEE Conference on Computer Vision and Pattern Recognition*, pages 633–641, 2017. [8](#)